analytical chemistry

pubs.acs.org/ac Article

Conformational Characterization of Peptides and Proteins by 193 nm Ultraviolet Photodissociation in the Collision Cell of a Trapped Ion Mobility Spectrometry-Time-of-Flight Mass Spectrometer

Jamie P. Butalewicz, Edwin E. Escobar, Christopher A. Wootton, Alina Theisen, Melvin A. Park, Erin H. Seeley, and Jennifer S. Brodbelt*

Cite This: *Anal. Chem.* 2024, 96, 16154−16161 Read Online

ACCESS | Metrics & More | Article Recommendations | Supporting Information

ABSTRACT: Ultraviolet photodissociation (UVPD) has been shown to be a versatile ion activation strategy for the characterization of peptides and intact proteins among other classes of biological molecules. Combining the high-performance mass spectrometry (MS/MS) capabilities of UVPD with the high-resolution separation of trapped ion mobility spectrometry (TIMS) presents an opportunity for enhanced structural elucidation of biological molecules. In the present work, we integrate a 193 nm excimer laser in a TIMS-time-of-flight (TIMS-TOF) mass spectrometer for UVPD in the collision cell and use it for the analysis of several mass-mobility-selected species of ubiquitin and myoglobin. The resultant data displayed differences in fragmentation that could be correlated with changes in protein conformation. Additionally, this mobility-resolved UVPD strategy was applied to collision-induced unfolded ions of ubiquitin to follow changes in fragmentation patterns relating to the extent of protein unfolding. This platform and methodology offer new opportunities for exploring how conformational variations are manifested in the fragmentation patterns of gas-phase ions.

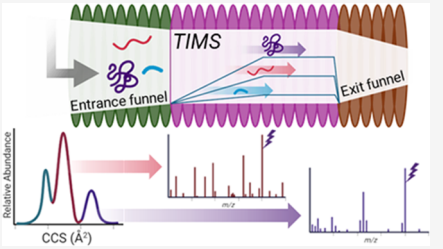

INTRODUCTION

Characterization of proteins at multiple levels, ranging from primary sequence and the ensemble of post-translational modifications to protein folding, conformation, and arrangement of subunits, plays a critical role in understanding complex cellular processes and biochemical pathways in living organisms.[1,2] The varying conformations that proteins can adopt directly influence their functional roles and interactions with cofactors, substrates, and many other biological molecules.[3,4] Characterizing these conformations presents significant challenges owing to their dynamic nature, influences from other molecules, and the transient nature of many structural states. Along with well-established biophysical methods such as X-ray crystallography,[5] cryo-electron microscopy,[6] and NMR spectroscopy,[7] mass spectrometry (MS) has emerged as a widely adopted analytical tool to elucidate protein structures,[8−10] decipher patterns of post-translational modifications (PTM),[11] and map protein−protein or protein−substrate interactions.[12,13] Coupling liquid chromatography (LC)[14] or ion mobility (IM) separations[15,16] with mass spectrometry can further enhance the number and range of different molecules that can be analyzed in complex biological systems.

Ion mobility-mass spectrometry (IM-MS) methods have gained popularity with the recent commercialization and implementation of techniques such as traveling wave ion mobility (TWIMS),[17] trapped ion mobility (TIMS),[18] cyclic ion mobility (cIM),[19] structures for lossless ion manipulation (SLIM),[20] and drift tube ion mobility (DTIMS)[15,16] on numerous MS platforms. IM offers the ability to separate peptides and proteins based on their molecular size, shape, and conformation, offering valuable insights into the protein folding and oligomerization events that may be induced by PTMs or ligand binding.[15] TIMS, cIM, and SLIM have demonstrated exceptionally high resolving powers, a performance metric that is particularly important for analyzing complex biological molecules with dynamic conformational landscapes.

The significant strides made in IM-MS techniques for the separation of peptide or protein conformations are complemented by MS/MS methods that allow specific conformations to be correlated with variations in ion fragmentation, thus revealing structural insights. Traditional ion activation for MS/MS is based on collision-induced dissociation (CID), typically generating readily assigned fragment ion types (b/y) from cleavages of the peptide or protein backbone.[21] The multiple collision, stepwise nature of collisional activation, may result in the heating and unfolding of the peptides or proteins and motivate the use of collisional activation as a means to induce

Received: May 23, 2024
Revised: September 24, 2024
Accepted: September 25, 2024
Published: October 4, 2024

the unfolding of proteins in an energy-controlled manner during ion mobility analysis, affording energy-dependent conformational fingerprints via a method termed collision-induced unfolding (CIU).[22] CIU offers insights into the structural dynamics and stability of proteins through interrogation of their unfolding pathways.[23,24] Other ion activation methods for MS/MS have also been coupled with IM separations, including electron-based methods (electron capture dissociation (ECD)[25,26] and electron transfer dissociation (ETD))[27] and surface-induced dissociation (SID).[28,29] Both IM-ECD[25,26] and IM-SID[28,29] methods have been used to characterize large, intact, native proteins and protein complexes.

Laser-based photodissociation methods have demonstrated their utility for examining the structural features of protein ions.[30−39] Ultraviolet photodissociation (UVPD) activates ions through high-energy photon absorption, unveiling primary sequence details and regions of higher-order structure.[40] UVPD is typically performed using a 193 or 213 nm laser, as the amide chromophores of the peptide backbone readily absorb in this range.[40] UVPD has been shown to directly probe gas-phase higher-order structures by generating *a/x, b/y*, and *c/z* fragment ion types.[40] While enabling greater sequence coverage of proteins, UVPD also offers insight into the localization of ligand binding sites and protein interfaces.[31,41]

Integrating UVPD with IM techniques offers the potential to expand strategies for the conformationally selective fragmentation of proteins. Several advancements have been made to couple IM and UVPD by modifying and adapting commercial instruments for photodissociation. For example, 266 nm UVPD[32,34] and 193 nm UVPD[42] have been implemented on quadrupole time-of-flight (Q-TOF) mass spectrometers equipped with TWIMS for IM separations. On this platform, UVPD occurred in the transfer cell prior to the TOF assembly, enabling ion trapping, accumulation, and fragmentation based on either m/z or arrival time.[32,42] Both 213 nm UVPD and 193 nm UVPD were implemented on TIMS-Q-TOF mass spectrometers equipped with high-resolution TIMS for IM separations.[43−45] These systems utilized a tandem-TIMS/MS configuration in which a supplementary TIMS funnel and ion trap were added to the front end of the instrument, allowing IM separation preceding and following the photodissociation event in the supplementary ion trap. Tandem-TIMS/MS configurations have demonstrated abilities to characterize protein conformations,[43,44,46,47] peptide assemblies,[48] various proteoforms,[46,49] and isomeric/isobaric species,[45] all capitalizing on the high resolving powers of TIMS.[18] IM-UVPD has been showcased for conformationally selective fragmentation of peptides, including angiotensin,[45] bradykinin,[42] and melittin,[34,42] and proteins,[50,51] including ubiquitin,[52−54] cytochrome c,[52,55] and myoglobin,[52] in each case demonstrating unique variations in fragment ions for different conformations.

Here, we report a new instrument configuration to perform 193 nm UVPD in the collision cell of a TIMS-TOF instrument. We report the conformational analysis of both peptides (angiotensin I) and proteins (ubiquitin and myoglobin) through mobility-selected fragmentation. Further, we showcase the combination of CIU with mobility-selected UVPD to monitor conformational changes as a function of protein unfolding.

METHODS AND MATERIALS

Materials. Ubiquitin from bovine erythrocytes and myoglobin from equine skeletal muscle were purchased from Sigma-Aldrich (St Louis, MO), and angiotensin I was purchased from Genscript (Piscataway, NJ). Each protein or peptide was dissolved in a 50/50 mixture of methanol/water with 1% formic acid to a final concentration of 10 μM. For any native MS experiments, each protein was dissolved in 100 mM ammonium acetate to a final concentration of 10 μM.

Instrumentation. A 193 nm excimer laser (Coherent, Santa Cruz, CA) was interfaced with the collision cell of a Bruker tims TOF fleX (Bruker, Billerica, MA) mass spectrometer using custom electronics for laser timing and triggering. The laser was positioned parallel to the mass spectrometer at a height equal to that of the center of the collision cell. A mirror held in place using a 90° kinematic mount (Thor Laboratories, Newton, NJ) was positioned in front of the laser window. An iris located between a mirror and the exit lens of the collision cell was used to trim the beam size to the appropriate diameter (Figure S1A). A CaF_2 window was installed on the outer vacuum housing of the instrument, adjacent to the orthogonal accelerator and entrance to the TOF region. An additional mirror was mounted on the orthogonal accelerator to direct the laser beam path through its center and into the collision cell. The exit lens of the collision cell was replaced with one containing a 1.5 mm diameter aperture, 1.0 mm greater than the standard lens aperture, to allow the introduction of a larger diameter laser beam. The laser was aligned through the collision cell while the system was at atmospheric pressure. The analytical quadrupole was removed during the laser alignment process to allow access to the entrance end of the collision cell.

Continuous accumulation of selected ion (CASI) waveforms was designed to allow m/z and mobility ion accumulation and isolation prior to UVPD. CASI waveforms were implemented on the collision cell to allow the accumulation and trapping of mobility-specific ions for subsequent UVPD. A general schematic of the waveforms is shown in Figure S1B, consisting primarily of two overlapping square waveforms with different offsets. Fully modifiable in a custom-built GUI, the ion accumulation and trapping times could be optimized based on the type of ions targeted in the TIMS separation. Larger ions required longer accumulation times (between 3000 and 5000 ms) in order to accumulate a sufficient population for UVPD, whereas peptides and other small molecules required much shorter accumulation times (<2000 ms). The trapping time was set based on the number of laser pulses used for each experiment; typically, 2 ms of trapping was employed for each 5 ns laser pulse used. The isolation of mobility-selected ions was based on an initial mobility sweep in which a small mobility window was incrementally stepped across a given mobility range to determine the mobility scan range for the desired ion population. Only ions within this small mobility range were accumulated and trapped.

Triggering of the excimer laser required the addition of a custom programmable circuit board (i.e., Arduino device) to receive direct outputs from the collision cell of the mass spectrometer. The entrance and exit lenses of the collision cell were monitored with an oscilloscope to determine the time period in which the ion population was accumulated versus that trapped within the collision cell. Custom electronic circuitry was used to simplify and reduce the voltage output

https://doi.org/10.1021/acs.analchem.4c02686
Anal. Chem. 2024, 96, 16154−16161

from these lenses for use with an Arduino Uno microcontroller board. Custom code was used to output a 5 V digital signal from the microcontroller board when the entrance lens was closed, signaling that ion accumulation was completed and the trapping phase had begun. A separate Arduino GUI was created to modulate the number of laser pulses per trapping event used in tandem with the 5 V digital signal to trigger the laser. An oscilloscope trace denoting the typical waveform outputs from the entrance and exit lenses, the processed entrance lens, and the resultant laser trigger is shown in Figure S1C.

Data Processing. All data was collected using Bruker timsControl 3.0 software and processed using Bruker DataAnalysis 6.0. Mobility-resolved UVPD profile data was deconvoluted using the SNAP algorithm with a quality factor threshold of 0.6 and relative and absolute intensity thresholds of 0.0 to ensure processing of the low abundance UVPD fragment ions. Instrument parameters and voltages used for native MS experiments are reported in Table S1. The generated mass list containing the "Isotopic Mass (Charge Deconv)" for all fragment ions was exported. As this "Isotopic Mass (Charge Deconv)" parameter was in the MH+ mode and not the neutral mass mode, processing in Excel was used to remove the extra hydrogen atom mass from each entry in the mass list. Subsequently, MS-TAFI was used to determine sequence coverage and fragmentation mapping using a 15 ppm error tolerance.[56] All UVPD data was collected in triplicate, and only fragments identified in at least two replicates were included for further analysis. All UVPD fragment ion identifications are shown in Table S2.

RESULTS AND DISCUSSION

193 nm UVPD Shows Complete Sequence Coverage of Peptide Angiotensin I. Peptide angiotensin I (sequence DRVYLHPFHL, monoisotopic mass 1295.68 Da) was used for the optimization of UVPD in the collision cell (Figure S2). The TIMS mobilogram of the 2+ and 3+ charge states is shown in Figure S2A. Utilizing the CASI waveforms, the 3+ charge state (m/z 432) was m/z isolated with a 5 Da isolation width and a wide mobility window, and the spectra obtained with the laser off and on (2 pulses, 2 mJ per pulse) are shown in Figure S3. With the laser off, the baseline around the precursor is relatively clean, with a few discernible ion peaks in addition to the isolated precursor.

Nineteen fragment ions are identified in the UVPD spectrum (Figure S3A), including six *a*-ions, four *b*-ions, four *x*-ions, two *y*-ions, and two *z*-ions (Table S2). The distribution of fragment ions generated by UVPD relative to the backbone positions that were cleaved is shown in Figure S3B. The prevalence of a-type fragment ions is well-known for UVPD.[40] Figure S4 illustrates the sequence coverage and signal-to-noise (S/N) of the precursor ion (a measure of precursor depletion) obtained using 1−5 laser pulses and 1.5−3.5 mJ per pulse. 100% sequence coverage was obtained using 2 mJ of laser energy and 2 pulses. To prevent overactivation of the ion population which leads to sequential fragmentation and production of internal fragment ions, two laser pulses at 2 mJ per pulse were selected for all subsequent experiments.

The corresponding results obtained based on CID are shown in Figure S5. For CID, complete sequence coverage of the peptide is achieved, generating 13 unique b- and y-type fragment ions. These initial benchmark results for TIMS-UVPD demonstrated the feasibility of using the modified collision cell and CASI waveforms for UVPD experiments.

Mobility-Resolved UVPD of Intact Proteins Resolves Multiple Conformers with Different Fragmentation Profiles. After optimization and assessment of TIMS-UVPD for peptides, mobility-resolved MS/MS experiments were performed for two proteins, ubiquitin and myoglobin, in order to evaluate the ability to obtain conformationally selective fragmentation profiles. Ubiquitin is an 8.6 kDa protein frequently studied owing to its diverse conformational variations as a function of charge state for both native-like and denatured forms of the protein.[57,58] Figure S6A shows the electrospray ionization (ESI) mass spectrum of ubiquitin sprayed from a methanol/water (denaturing conditions), and Figure 1A displays mobilograms of the three most abundant

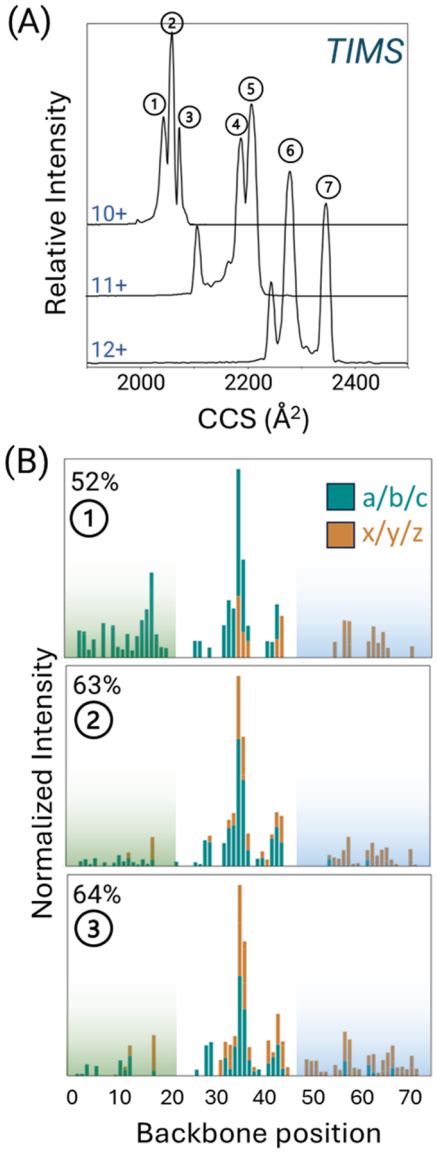

Figure 1. (A) TIMS mobilogram for the 10+−12+ charge states of ubiquitin. Circled numbers in the mobilogram correspond to peaks selected for the mobility-resolved UVPD. (B) Backbone cleavage maps constructed based on fragment ion abundances produced by UVPD of the three mobility-separated peaks of the 10+ charge state are shown in part (A). The abundances of fragment ions are mapped according to the backbone cleavage site from which they originate.

https://doi.org/10.1021/acs.analchem.4c02686
Anal. Chem. 2024, 96, 16154−16161

charge states (10+, 11+, 12+). Each of the charge states exhibits the presence of at least three abundant and distinctive peaks in the mobilograms, with those from the 11+ and 12+ charge states being more highly resolved than those of the 10+ charge state. These mobility-separated peaks align well with profiles reported in prior IM studies of ubiquitin.[52,57,59,60]

After mobility isolation, UVPD was performed on each of the three labeled peaks in Figure 1A for the 10+ charge state. The resulting sequence maps are shown in Figure S6B. Conformer 1 was centered at around 2040 Å^2 and was the smallest (most compact) of the three conformations. UVPD resulted in 52% sequence coverage, with 48 fragments identified. Conformer 2 was centered at around 2060 Å^2, yielding a sequence coverage of 63% with 75 fragments identified. Conformer 3 was centered at around 2080 Å^2, generating 64% sequence coverage and 88 identified fragment ions.

UVPD has been used previously to infer secondary and tertiary structural information about proteins owing to the preferential production of fragment ions from regions that are less stabilized by noncovalent interactions.[40] It is surmised that fragment ions are not as readily released upon backbone cleavages that occur in regions involved in networks of intramolecular interactions, suppressing the abundances of those fragment ions. Thus, variation in the secondary and tertiary structural features of the proteins may account for some of the variation in the abundances of fragment ions produced by cleavages throughout the protein backbone. Figure 1B shows backbone cleavage maps based on the abundances of N-terminal ions (*a*/*b*/*c* fragment ions) and C-terminal ions (*x*/*y*/*z* fragment ions) originating from cleavages at each backbone position for each of the three mobility-separated features of the 10+ charge state of ubiquitin. Conformer 1 generated somewhat lower sequence coverage than the other two conformers, an outcome attributed to its more compact conformation and smaller CCS that may impede more extensive fragmentation. In particular, fragmentation in the C-terminal region (spanning residues 47−76, shaded in blue in Figure 1B) of conformer 1 is reduced relative to the other two conformers, while the fragmentation in the N-terminal region (spanning residues 1−20, shaded in green) is enhanced in conformer 1 relative to the other two conformers. These localized differences in fragmentation may reflect regional variations in the conformer structures, specifically related to the orientation of the C-terminal tail region. Examination of the secondary structural map of the A-state of ubiquitin (Figure S6C) indicates that the C-terminal region contains an unstructured loop (spanning residues 71 to 76), which could potentially engage in intermolecular interactions with other regions of the protein.

In contrast to the fragmentation of conformer 1, conformer 3 displays more extensive fragmentation of the C-terminal region of the protein and less extensive fragmentation of the N-terminal region, suggesting that the C-terminal loop may be more elongated while the N-terminal region may be reoriented with more intramolecular interactions. For all three conformers examined for the 10+ charge state, the central region spanning residues G35−Q40 of the protein shows extensive fragmentation. In the secondary structural map of the A-state of ubiquitin seen in Figure S6C, these residues comprise a relatively unstructured loop region of the protein containing two proline residues. The higher flexibility of this structural region and the known preferential backbone cleavage adjacent to Pro residues for UVPD[52,54,59] may contribute to the efficient fragmentation of this segment for all three conformations.

UVPD was also performed on the mobility-separated conformations of the 11+ and 12+ charge states of ubiquitin (Figure 1A), and the resulting sequence coverage and backbone cleavage maps are shown in Figure S7. For both charge states, there are variations in the fragmentation based on the selected conformation. The 11+ charge state generated 68 fragments with 59% sequence coverage for the smaller conformation peak 4 and 101 fragments with 68% sequence coverage for the larger conformer peak 5 (Table S2). The 12+ charge state generated 94 fragments with 69% sequence coverage for the smaller conformation peak 6 and 93 fragments with 72% sequence coverage for the larger conformer peak 7 (Table S2). Similarly to the 10+ charge state, the smaller conformations of the 11+ and 12+ charge states (conformers 4 and 6) show enhanced fragmentation of the N-terminal region, whereas the larger conformers (conformers 5 and 7) show more extensive coverage of the C-terminal region of the protein. In addition, fragmentation of the central sequence section spanning G35−Q40 is notably enhanced for conformers 5, 6, and 7. In addition to the impact of the charge state, some of these variations in fragmentation may be related to differences in the network of stabilizing intramolecular interactions that vary for different conformations and influence the production of fragment ions. Specifically, conformational variations directly related to *cis*/*trans* isomerization of proline residues are of particular interest with continued improvements in instrumentation and subsequently UVPD sequence coverage.

The conformational diversity of myoglobin (16.9 kDa) has also been extensively studied and demonstrates a great variety of conformational variations across its charge states.[52,57,61] The ESI mass spectrum of myoglobin is shown in Figure S8. The 23+ charge state was selected for ion mobility and UVPD analysis due to the structural complexity seen in the TIMS mobilogram (Figure 2A). The ion mobilogram is centered at around 5250 Å^2 and displays three overlapping peaks, each highlighted to indicate the specific mobility windows isolated for UVPD (Figure 2A). Figure 2B shows the UVPD spectra collected for the slice representing the most elongated forms (largest collision cross section). The resulting sequence coverage maps obtained for the ions populating the more compact and more extended conformational windows are shown in Figure 2C, and the abundances of fragment ions based on backbone cleavage sites are shown in Figure S9. UVPD of the more compact conformer generated 31 fragments and 19% sequence coverage; 57 fragment ions and 36% sequence coverage were obtained for the larger conformer. A comparison of the two sequence maps shows that while the C- and N-terminal regions yielded somewhat similar fragmentation, the central sequence section (shaded in each of the maps in Figures 2C and S9) generated 17 more fragment ions for the larger conformer. This outcome is consistent with the prediction that larger, more elongated conformers have fewer intramolecular interactions that suppress the release of fragment ions.

The trends of escalating sequence coverage and number of identified fragment ions for more elongated conformers remain consistent across various conformations for the 11+ and 12+ charge states of ubiquitin, as well as the 23+ charge state of myoglobin. These examples demonstrate the ability to obtain high mobility resolution and photodissociation of different

https://doi.org/10.1021/acs.analchem.4c02686
Anal. Chem. 2024, 96, 16154−16161

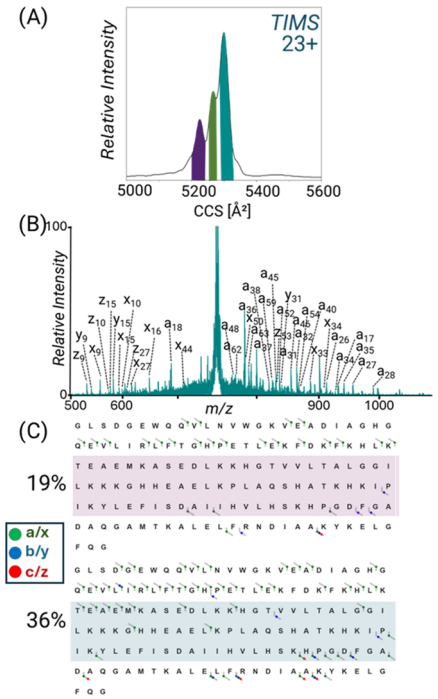

Figure 2. (A) TIMS mobilogram of the 23+ charge state of myoglobin, with each color representing a different conformational section that was mobility isolated for UVPD. (B) UVPD spectrum of a more extended (teal) conformation with various fragment ions labeled. (C) Sequence coverage maps for two conformers (more compact and more extended) with the shaded regions displaying significant differences in fragmentation. Backbone cleavage sites are represented by diagonal flags that are color-coded based on the fragment ion type.

conformations of proteins in the same charge state, highlighting the performance of the integrated strategy.

Collision-Induced Unfolding (CIU) of Native-Like Ubiquitin Reveals Five Distinct Conformers, Each Showing Increased Fragmentation in the Central Region of the Protein. Recent studies have demonstrated that TIMS-TOF mass spectrometers can be tuned to preserve native-like protein structures[62−64] throughout the ionization, TIMS, and MS analysis steps, thus allowing subsequent structural analysis.[65−67] The capability to perform CIU allows additional insight into conformational changes and unfolding, as proteins are incrementally destabilized by collisional activation. Figure S10 shows the mass spectrum obtained for a solution containing 10 uM ubiquitin and 100 mM ammonium acetate, the resulting mobilogram of the 6+ charge state, and the corresponding crystal structure of native ubiquitin (PDB: 1UBQ). The mobilogram and CCS values align well with prior studies of the native-like 6+ charge state of ubiquitin,[52,57,66] showing multiple conformations with the greatest intensity centered at around 1200 Å^2, supporting the preservation of its structure on the TIMS-TOF platform.

For the TIMS-TOF system, it has been previously shown that the Δ6 potential of the TIMS cell can be varied to induce protein unfolding in a manner akin to conventional CIU.[66,68] This potential is responsible for the acceleration of ions out of the accumulation region of the TIMS cell and into the analysis region containing a voltage gradient for mobility separation. Low Δ6 values (under 50 V) typically result in little activation of the ions and thus cause marginal or no change in ion mobility or collision cross section. However, when the Δ6 voltage is increased beyond 100 V, significant changes are observed in the mobilogram, indicative of protein unfolding. Figure 3A shows the CIU plot for the 6+ charge state of ubiquitin as a function of the Δ6 voltage. Several distinct features are evident, notably those that emerge around 100 V. As illustrated in the mobilograms that correspond to the three boxed regions of the CIU diagram (Figure 3B), at low energy, ubiquitin features at least two broad unresolved peaks (between 1000 and 1400 Å^2). However, as the delta voltage is increased (higher collision energy), the low CCS bimodal peak disappears, presumably merging into one broad peak centered at around 1350 Å^2. Further energy deposition results in the appearance of another peak centered at around 1550 Å^2. Upon comparison of the mobilograms in Figure 3B to those reported in ref66, there is evidence for some degree of unfolding even prior to variation of the delta voltage in the present study. Moreover, the CCS values in the present study are not identical to those reported in ref66. These differences may be related to some activation that occurs owing to the long multisecond accumulation time and the mobility calibration used in the present study.

The variation in CCS values provides insight into the unfolding of the protein, and additional information can be derived by examining the fragmentation of the protein throughout the mobilogram profile.[69] UVPD was performed on the populations of ions constituting the four highlighted regions of the mobilograms shown in Figure 3B, resulting in the four backbone cleavage plots shown in Figure 3C and sequence coverage maps shown in Figure S11. For the ions representing the two distinctive conformational bands obtained at no-to-low Δ6 potential, the sequence coverage was greater for the conformer with the larger CCS (shaded blue), generating five additional fragment ions and a 7% increase in coverage. The overall sequence coverage is significantly lower than the coverage obtained for the 10+ to 12+ charge states of ubiquitin described earlier, an outcome consistent with the suppression of fragmentation expected for compact structures constrained by more intramolecular interactions. UVPD of the ions populating the conformational window generated when the Δ6 potential was increased to 100 V (shaded in green) resulted in a slight 1% increase in sequence coverage based on the identification of five additional fragment ions and yielded a fragmentation map similar to the one observed for the ones obtained when the Δ6 potential was 25 V.

When the Δ6 potential exceeds 100 V, a notable transition occurs in the CIU plot, going from a single broad conformational band to a narrower band, corresponding to a larger CCS value centered at around 1550 Å^2. UVPD was acquired for the ions in this mobility band (shaded in lavender in Figure 3B), resulting in 36% sequence coverage and a much broader distribution of fragment ions based on the backbone cleavage map in Figure 3C. There is substantially more fragmentation in the central region of the protein sequence, suggesting a significant unfolding of the protein. It is possible that analyzing even narrower slices of the ion population throughout the mobilogram would show the incremental shifts and changes in fragmentation in more detail.

CONCLUSIONS

We have demonstrated a new TIMS-TOF-UVPD configuration in which a 193 nm UVPD is performed in the collision

https://doi.org/10.1021/acs.analchem.4c02686
Anal. Chem. 2024, 96, 16154−16161

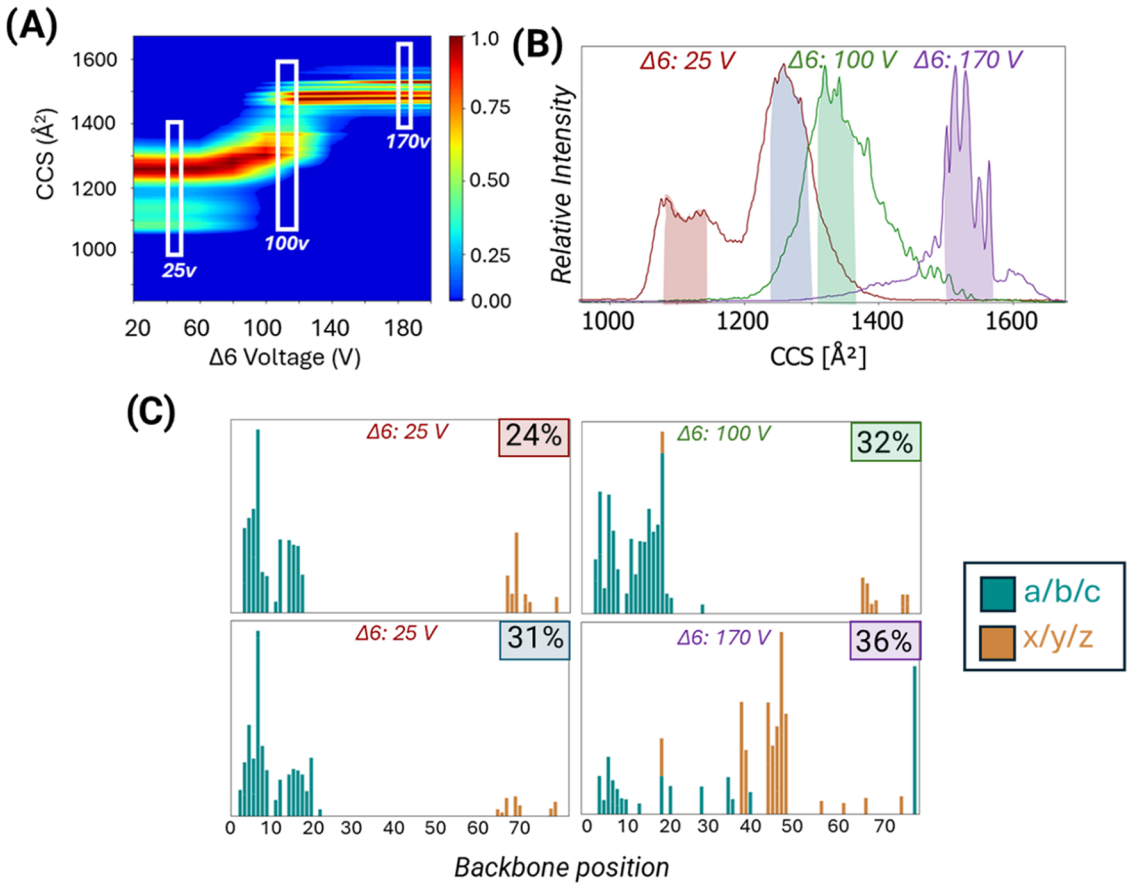

Figure 3. (A) CIU plot for the 6+ charge state of ubiquitin when the Δ6 voltage is varied from 0 to 200 V (system maximum). (B) Mobilograms that correspond to the three boxed regions of the CIU plot. The four shaded regions are those for which the populations of ions were subjected to UVPD. (C) Backbone cleavage maps constructed based on fragment ion abundances produced by UVPD of the four mobility-separated populations of ubiquitin.

cell. CASI methods were used for ion accumulation and m/z isolation for peptides and proteins. Mobility selection was demonstrated for ubiquitin and myoglobin, each of which exhibited conformational profiles, suggesting variations in the sizes of ions. Ions in each conformational band generated distinct UVPD fragmentation patterns that reflected a difference in the elongation of the protein, presumably related to the degree of noncovalent interactions. CIU curves were generated based on increasing the Δ6 voltage applied to the TIMS cell. As the voltage increased, the corresponding degree of fragmentation of the protein increased, which is consistent with protein unfolding. Fragmentation patterns acquired as a function of the applied voltage revealed an increasing level of backbone fragmentation originating from more interior regions of the protein. The benchmark results reported here establish a framework for the broader adoption of the TIMS-TOF-UVPD strategy for examining correlating variations in fragmentation with conformational changes of larger proteins.

■ ASSOCIATED CONTENT

Supporting Information

The Supporting Information is available free of charge at https://pubs.acs.org/doi/10.1021/acs.analchem.4c02686.

Tables of experimental parameters and UVPD fragment ion identifications (XLSX)

Additional figures showing instrument schematic; TIMS mobilograms; MS1, UVPD and CID mass spectra; plots of sequence coverage versus number of laser pulses and laser power; and backbone cleavage maps (PDF)

■ AUTHOR INFORMATION

Corresponding Author

Jennifer S. Brodbelt − *Department of Chemistry, The University of Texas at Austin, Austin, Texas 78712, United States;* orcid.org/0000-0003-3207-0217; Email: jbrodbelt@cm.utexas.edu

Authors

Jamie P. Butalewicz − *Department of Chemistry, The University of Texas at Austin, Austin, Texas 78712, United States*

Edwin E. Escobar − *Department of Chemistry, The University of Texas at Austin, Austin, Texas 78712, United States;* orcid.org/0000-0002-0086-6264

Christopher A. Wootton − *Bruker Daltonics GmbH & Co. KG, Bremen 28359, Germany*

Alina Theisen − *Bruker Daltonics GmbH & Co. KG, Bremen 28359, Germany*

Melvin A. Park − *Bruker Daltonics Inc., Billerica, Massachusetts 01821, United States;* orcid.org/0009-0004-1448-2896

Erin H. Seeley − *Department of Chemistry, The University of Texas at Austin, Austin, Texas 78712, United States;* orcid.org/0000-0002-8000-5754

https://doi.org/10.1021/acs.analchem.4c02686
Anal. Chem. 2024, 96, 16154−16161

Complete contact information is available at:
https://pubs.acs.org/10.1021/acs.analchem.4c02686

Notes

The authors declare the following competing financial interest(s): C.A.W., A.T., and M.A.P. are employees of Bruker Daltonics Inc., the developers of the tims-TOF mass spectrometer used for the study.

■ ACKNOWLEDGMENTS

We acknowledge the following funding sources: NSF (Grant CHE-2203602), the Welch Foundation (Grant F-1155), and the Cancer Prevention and Research Institute of Texas (Award RP190617).

■ REFERENCES

(1) Aebersold, R.; Agar, J. N.; Amster, I. J.; et al. *Nat. Chem. Biol.* **2018**, *14* (3), 206−214.
(2) Clemmer, D. E.; Russell, D. H.; Williams, E. R. *Acc. Chem. Res.* **2017**, *50* (3), 556−560.
(3) Dill, K. A.; MacCallum, J. L. *Science* **2012**, *338* (6110), 1042−1046.
(4) Wrabl, J. O.; Gu, J.; Liu, T.; Schrank, T. P.; Whitten, S. T.; Hilser, V. J. *Biophys. Chem.* **2011**, *159* (1), 129−141.
(5) Shi, Y. *Cell* **2014**, *159* (5), 995−1014.
(6) Danev, R.; Yanagisawa, H.; Kikkawa, M. *Trends Biochem. Sci.* **2019**, *44* (10), 837−848.
(7) Ziarek, J. J.; Baptista, D.; Wagner, G. *J. Mol. Med.* **2018**, *96* (1), 1−8.
(8) Leney, A. C.; Heck, A. J. R. *J. Am. Soc. Mass Spectrom.* **2017**, *28* (1), 5−13.
(9) Tamara, S.; den Boer, M. A.; Heck, A. J. R. *Chem. Rev.* **2022**, *122* (8), 7269−7326.
(10) Karch, K. R.; Snyder, D. T.; Harvey, S. R.; Wysocki, V. H. *Annu. Rev. Biophys.* **2022**, *51*, 157−179.
(11) Schaffer, L. V.; Millikin, R. J.; Miller, R. M.; Anderson, L. C.; Fellers, R. T.; Ge, Y.; Kelleher, N. L.; LeDuc, R. D.; Liu, X.; Payne, S. H.; Sun, L.; Thomas, P. M.; Tucholski, T.; Wang, Z.; Wu, S.; Wu, Z.; Yu, D.; Shortreed, M. R.; Smith, L. M. *Proteomics* **2019**, *19* (10), No. 1800361.
(12) Sinz, A. *Angew. Chem., Int. Ed.* **2018**, *57* (22), 6390−6396.
(13) Richards, A. L.; Eckhardt, M.; Krogan, N. J. *Mol. Syst. Biol.* **2021**, *17* (1), No. e8792.
(14) Chen, G.; Pramanik, B. N. *Drug Discovery Today* **2009**, *14* (9), 465−471.
(15) Dodds, J. N.; Baker, E. S. *J. Am. Soc. Mass Spectrom.* **2019**, *30* (11), 2185−2195.
(16) Christofi, E.; Barran, P. *Chem. Rev.* **2023**, *123* (6), 2902−2949.
(17) Shvartsburg, A. A.; Smith, R. D. *Anal. Chem.* **2008**, *80* (24), 9689−9699.
(18) Michelmann, K.; Silveira, J. A.; Ridgeway, M. E.; Park, M. A. *J. Am. Soc. Mass Spectrom.* **2015**, *26* (1), 14−24.
(19) Giles, K.; Ujma, J.; Wildgoose, J.; Pringle, S.; Richardson, K.; Langridge, D.; Green, M. *Anal. Chem.* **2019**, *91* (13), 8564−8573.
(20) Hamid, A. M.; Ibrahim, Y. M.; Garimella, S. V. B.; Webb, I. K.; Deng, L.; Chen, T.-C.; Anderson, G. A.; Prost, S. A.; Norheim, R. V.; Tolmachev, A. V.; Smith, R. D. *Anal. Chem.* **2015**, *87* (22), 11301−11308.
(21) Wells, J. M.; McLuckey, S. A. Collision-Induced Dissociation (CID) of Peptides and Proteins. In *Methods in Enzymology*; Academic Press, 2005; Vol. *402*, pp 148−185.
(22) Dixit, S. M.; Polasky, D. A.; Ruotolo, B. T. *Curr. Opin. Chem. Biol.* **2018**, *42*, 93−100.
(23) Hopper, J. T. S.; Oldham, N. J. *J. Am. Soc. Mass Spectrom.* **2009**, *20* (10), 1851−1858.
(24) Polasky, D. A.; Dixit, S. M.; Fantin, S. M.; Ruotolo, B. T. *Anal. Chem.* **2019**, *91* (4), 3147−3155.
(25) Wang, H.; Eschweiler, J.; Cui, W.; Zhang, H.; Frieden, C.; Ruotolo, B. T.; Gross, M. L. *J. Am. Soc. Mass Spectrom.* **2019**, *30* (5), 876−885.
(26) Gadkari, V. V.; Ramírez, C. R.; Vallejo, D. D.; Kurulugama, R. T.; Fjeldsted, J. C.; Ruotolo, B. T. *Anal. Chem.* **2020**, *92* (23), 15489−15496.
(27) Shaw, J. B.; Cooper-Shepherd, D. A.; Hewitt, D.; Wildgoose, J. L.; Beckman, J. S.; Langridge, J. I.; Voinov, V. G. *Anal. Chem.* **2022**, *94* (9), 3888−3896.
(28) Snyder, D. T.; Jones, B. J.; Lin, Y.-F.; Cooper-Shepherd, D. A.; Hewitt, D.; Wildgoose, J.; Brown, J. M.; Langridge, J.; Wysocki, V. H. *Analyst* **2021**, *146* (22), 6861−6873.
(29) Harvey, S. R.; Seffernick, J. T.; Quintyn, R. S.; Song, Y.; Ju, Y.; Yan, J.; Sahasrabuddhe, A. N.; Norris, A.; Zhou, M.; Behrman, E. J.; Lindert, S.; Wysocki, V. H. *Proc. Natl. Acad. Sci. U.S.A.* **2019**, *116* (17), 8143−8148.
(30) Zhou, M.; Lantz, C.; A Brown, K.; Ge, Y.; Paša-Tolić, L.; A Loo, J.; Lermyte, F. *Chem. Sci.* **2020**, *11* (48), 12918−12936.
(31) O'Brien, J. P.; Li, W.; Zhang, Y.; Brodbelt, J. S. *J. Am. Chem. Soc.* **2014**, *136* (37), 12920−12928.
(32) Bellina, B.; Brown, J. M.; Ujma, J.; Murray, P.; Giles, K.; Morris, M.; Compagnon, I.; Barran, P. E. *Analyst* **2014**, *139* (24), 6348−6351.
(33) Shaw, J. B.; Li, W.; Holden, D. D.; Zhang, Y.; Griep-Raming, J.; Fellers, R. T.; Early, B. P.; Thomas, P. M.; Kelleher, N. L.; Brodbelt, J. S. *J. Am. Chem. Soc.* **2013**, *135* (34), 12646−12651.
(34) Theisen, A.; Yan, B.; Brown, J. M.; Morris, M.; Bellina, B.; Barran, P. E. *Anal. Chem.* **2016**, *88* (20), 9964−9971.
(35) Ly, T.; Julian, R. R. *Angew. Chem., Int. Ed.* **2009**, *48* (39), 7130−7137.
(36) Luo, P.; Liu, Z.; Lai, C.; Jin, Z.; Wang, M.; Zhao, H.; Liu, Y.; Zhang, W.; Wang, X.; Xiao, C.; Yang, X.; Wang, F. *J. Am. Chem. Soc.* **2024**, *146* (13), 8832−8838.
(37) Shaw, J. B.; Liu, W.; Vasil'ev, Y. V.; Bracken, C. C.; Malhan, N.; Guthals, A.; Beckman, J. S.; Voinov, V. G. *Anal. Chem.* **2020**, *92* (1), 766−773.
(38) Tamara, S.; Dyachenko, A.; Fort, K. L.; Makarov, A. A.; Scheltema, R. A.; Heck, A. J. R. *J. Am. Chem. Soc.* **2016**, *138* (34), 10860−10868.
(39) Halim, M. A.; Girod, M.; MacAleese, L.; Lemoine, J.; Antoine, R.; Dugourd, P. *J. Am. Soc. Mass Spectrom.* **2016**, *27* (9), 1435−1442.
(40) Brodbelt, J. S.; Morrison, L. J.; Santos, I. *Chem. Rev.* **2020**, *120* (7), 3328−3380.
(41) Sipe, S. N.; Lancaster, E. B.; Butalewicz, J. P.; Whitman, C. P.; Brodbelt, J. S. *J. Am. Chem. Soc.* **2022**, *144* (27), 12299−12309.
(42) Stiving, A. Q.; Harvey, S. R.; Jones, B. J.; Bellina, B.; Brown, J. M.; Barran, P. E.; Wysocki, V. H. *J. Am. Soc. Mass Spectrom.* **2020**, *31* (11), 2313−2320.
(43) Liu, F. C.; Ridgeway, M. E.; Winfred, J. S. R. V.; Polfer, N. C.; Lee, J.; Theisen, A.; Wootton, C. A.; Park, M. A.; Bleiholder, C. *Rapid Commun. Mass Spectrom.* **2021**, *35* (22), No. e9192.
(44) Liu, F. C.; Ridgeway, M. E.; Wootton, C. A.; Theisen, A.; Panczyk, E. M.; Meier, F.; Park, M. A.; Bleiholder, C. *J. Am. Soc. Mass Spectrom.* **2023**, *34* (10), 2232−2246.
(45) Miller, S. A.; Fouque, K. J. D.; Ridgeway, M. E.; Park, M. A.; Fernandez-Lima, F. *J. Am. Soc. Mass Spectrom.* **2022**, *33* (7), 1267−1275.
(46) Liu, F. C.; Cropley, T. C.; Ridgeway, M. E.; Park, M. A.; Bleiholder, C. *Anal. Chem.* **2020**, *92* (6), 4459−4467.
(47) Cropley, T. C.; Liu, F. C.; Chai, M.; Bush, M. F.; Bleiholder, C. *J. Am. Chem. Soc.* **2024**, *146* (16), 11115−11125.
(48) Kirk, S. R.; Liu, F. C.; Cropley, T. C.; Carlock, H. R.; Bleiholder, C. *J. Am. Soc. Mass Spectrom.* **2019**, *30* (7), 1204−1212.
(49) Fouque, K. J. D.; Kaplan, D.; Voinov, V. G.; Holck, F. H. V.; Jensen, O. N.; Fernandez-Lima, F. *Anal. Chem.* **2021**, *93* (27), 9575−9582.
(50) Miller, S. A.; Fouque, K. J. D.; Hard, E. R.; Balana, A. T.; Kaplan, D.; Voinov, V. G.; Ridgeway, M. E.; Park, M. A.; Anderson, G. A.; Pratt, M. R.; Fernandez-Lima, F. *Anal. Chem.* **2023**, *95* (49), 18039−18045.

(51) Fouque, K. J. D.; Miller, S. A.; Pham, K.; Bhanu, N. V.; Cintron-Diaz, Y. L.; Leyva, D.; Kaplan, D.; Voinov, V. G.; Ridgeway, M. E.; Park, M. A.; Garcia, B. A.; Fernandez-Lima, F. *Anal. Chem.* **2022**, *94* (44), 15377−15385.
(52) Theisen, A.; Black, R.; Corinti, D.; Brown, J. M.; Bellina, B.; Barran, P. E. *J. Am. Soc. Mass Spectrom.* **2019**, *30* (1), 24−33.
(53) Warnke, S.; von Helden, G.; Pagel, K. *Proteomics* **2015**, *15* (16), 2804−2812.
(54) Warnke, S.; Baldauf, C.; Bowers, M. T.; Pagel, K.; Helden, G. *J. Am. Chem. Soc.* **2014**, *136* (29), 10308−10314.
(55) Black, R.; Barkhanskiy, A.; Ramakers, L. A. I.; Theisen, A.; Brown, J. M.; Bellina, B.; Trivedi, D. K.; Barran, P. E. *Int. J. Mass Spectrom.* **2021**, *464*, No. 116588.
(56) Juetten, K. J.; Brodbelt, J. S. *J. Proteome Res.* **2023**, *22* (2), 546−550.
(57) May, J. C.; Jurneczko, E.; Stow, S. M.; Kratochvil, I.; Kalkhof, S.; McLean, J. A. *Int. J. Mass Spectrom.* **2018**, *427*, 79−90.
(58) El-Baba, T. J.; Woodall, D. W.; Raab, S. A.; Fuller, D. R.; Laganowsky, A.; Russell, D. H.; Clemmer, D. E. *J. Am. Chem. Soc.* **2017**, *139* (18), 6306−6309.
(59) Shi, H.; Pierson, N. A.; Valentine, S. J.; Clemmer, D. E. *J. Phys. Chem. B* **2012**, *116* (10), 3344−3352.
(60) Shi, H.; Clemmer, D. E. *J. Phys. Chem. B* **2014**, *118* (13), 3498−3506.
(61) Woodall, D. W.; Henderson, L. W.; Raab, S. A.; Honma, K.; Clemmer, D. E. *J. Am. Soc. Mass Spectrom.* **2021**, *32* (1), 64−72.
(62) Ridgeway, M. E.; Silveira, J. A.; Meier, J. E.; Park, M. A. *Analyst* **2015**, *140* (20), 6964−6972.
(63) Liu, F. C.; Kirk, S. R.; Bleiholder, C. *Analyst* **2016**, *141* (12), 3722−3730.
(64) Bleiholder, C.; Liu, F. C.; Chai, M. *Anal. Chem.* **2020**, *92* (24), 16329−16333.
(65) Panczyk, E.; Lin, Y.-F.; Snyder, D.; Liu, F.; Ridgeway, M.; Park, M.; Bleiholder, C.; Wysocki, V. Evaluation of a Bruker timsTOF Pro for Native Mass Spectrometry *ChemRxiv* 2023 DOI: 10.26434/chemrxiv-2021-qr78t-v2.
(66) Borotto, N. B.; Osho, K. E.; Richards, T. K.; Graham, K. A. *J. Am. Soc. Mass Spectrom.* **2022**, *33* (1), 83−89.
(67) Fouque, K. J. D.; Garabedian, A.; Leng, F.; Tse-Dinh, Y.-C.; Ridgeway, M. E.; Park, M. A.; Fernandez-Lima, F. *Anal. Chem.* **2021**, *93* (5), 2933−2941.
(68) Graham, K. A.; Lawlor, C. F.; Borotto, N. B. *Analyst* **2023**, *148* (7), 1534−1542.
(69) Borotto, N. B.; Graham, K. A. *Anal. Chem.* **2021**, *93* (29), 9959−9964.

https://doi.org/10.1021/acs.analchem.4c02686
Anal. Chem. 2024, 96, 16154−16161